Optics Letters

Optical lattice induced by angular momentum and polygonal plasmonic mode

Yu Wang, Yuntao Xu, Xue Feng,* Peng Zhao, Fang Liu, Kaiyu Cui, Wei Zhang, and Yidong Huang

Department of Electronic Engineering, Tsinghua National Laboratory for Information Science and Technology, Tsinghua University, Beijing, China
**Corresponding author: x-feng@tsinghua.edu.cn*

Received 12 January 2016; revised 26 February 2016; accepted 2 March 2016; posted 2 March 2016 (Doc. ID 256873); published 22 March 2016

A series of plasmonic devices are proposed to generate multipatterned and two-dimensional optical lattices with or without helicity. Both the spin and orbital angular momentum of incident beam together with the excited polygonal plasmonic mode contribute to the formation of optical lattices due to the spin-orbit coupling. The impact of the mode property of incident beams on lattice pattern deforming is also discussed. Due to the compactness and flexible tunability, we believe that this work would facilitate the utilization of optical lattices in various on-chip applications.

OCIS codes: (050.4865) Optical vortices; (240.6680) Surface plasmons; (260.3160) Interference; (260.6042) Singular optics.

http://dx.doi.org/10.1364/OL.41.001478

As a periodic field potential, the optical lattice is a fundamental platform for the study of many branches of physics [1,2]. An optical lattice is usually formed by the interference of two or more coherent waves and has been demonstrated as a kind of light-sculpting technology [3,4]. In fact, it is essential for sculpting the phase profile of a light beam [5] as well as the intensity. Specifically, light beams with spiral phase fronts carry orbital angular momentum (OAM) and are known as optical vortices [6–8]. Optical vortices have been used in various applications, such as particle manipulation and classic/quantum information [9–11]. Thus it is quite attractive to combine the vortex features with an optical lattice to form a new branch of vortex lattice [12–14]. With respect to the traditional lattice without helicity, which mainly traps and stabilizes, a vortex lattice with helicity has more potential, such as microfluidic sorting [15,16] and particle-enhanced diffusions [17].

Though equipped with great utility, the state of the art methods for generating optical lattices mainly rely on spatial optics. Therefore, there are limits due to the complexity and footprint of the whole optical system. Fortunately, it is possible to implement a complicated optical system on a tiny photonic chip with integration technology, and it is exciting to see that optical lattices have been realized by semiconductor microcavities [18], atom chips [19], and plasmonic devices [20] experimentally. As plasmonics is inherently a near field on a metal surface [21], it is a perfect vehicle for light–matter interactions [22] with intense local energy. In this Letter, we propose an on-chip scheme to generate multipatterned and two-dimensional optical lattices with and without helicity. The generated optical lattice is induced by spin angular momentum (SAM) and OAM carried by incident beams, as well as the excited polygonal plasmonic mode.

As optical lattices are the result of multibeam interference, several slits are etched on a 200 nm gold membrane to excite multicoherent plasmonic waves. Specifically, the device is composed of N-edge polygonal-shaped slits, for both easy design and fabrication. In Fig. 1, a hexagon-shaped device ($N = 6$) is shown as an example. The incident beam ($\mathbf{E}_{s,l}$) is of circular polarized Laguerre–Gaussian (LG) mode with a wavelength of around 633 nm, while the carried SAM and OAM are quantified as $s\hbar$ ($s = \pm 1$) and $l\hbar$ ($l = 0, \pm 1, \pm 2, \ldots$) per photon [23], respectively. With a wave vector matching condition, a momentum compensation is necessary to excite a plasmonic wave [20]. As a slit usually supports a very broad range of wave

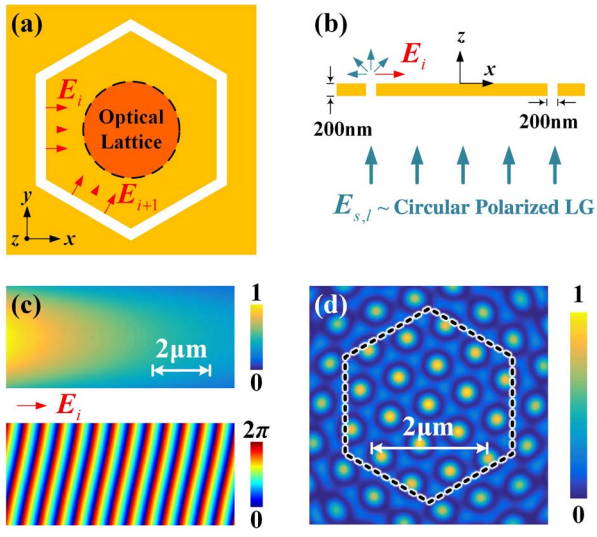

Fig. 1. (a) Top and (b) lateral view of a hexagon-shaped device ($N = 6$). The incident circular polarized LG beam carries both SAM and OAM; (c) top view of intensity pattern and phase (of $\boldsymbol{E}_z$) profile of an excited plasmonic wave from one slit; (d) intensity pattern of a certain optical lattice generated.

vectors due to its sharp corners, surface plasmonic waves ($\mathbf{E}_i$, $i = 1 \sim N$) would be excited at each slit by automatically selecting the appropriate wave vector and then propragating toward the center, superposing as a polygonal plasmonic mode naturally. As a result of interference, an optical lattice would be generated in the center of the hexagon-shaped device, as marked by the dashed circle in Fig. 1(a).

The electric field expression for an excited surface plasmonic wave ($z > 0$) propagating along the x axis could be written as [21]

$$\boldsymbol{E}_{\mathrm{sp}} = \begin{bmatrix} E_{i,\perp} \\ E_{i,\parallel} \\ E_{i,z} \end{bmatrix} \propto \begin{bmatrix} -k_z \\ 0 \\ k_{\mathrm{sp}} \end{bmatrix} e^{j(\omega t - k_{\mathrm{sp}} x + k_z z)}. \tag{1}$$

It is fundamentally composed of a slit-perpendicular component and a z component while the slit-parallel component is zero, due to the TM polarization of plasmonic waves. Parameters are calculated with gold constants from Ref. [24], and wave vector k depicts the intensity decaying in the z direction. The plasmonic wave vector is described by k_{sp} with resonant wavelength ~600 nm. As $k_z \ll k_{\mathrm{sp}}$, the z component dominates in the near field [21].

The incident LG beam with circular polarization is given as [23]

$$\boldsymbol{E}_{s,l} \propto \left(\frac{\sqrt{2}r}{w(z)}\right)^{|l|} L_p^{|l|}\left(\frac{2r^2}{w(z)^2}\right) e^{-\frac{r^2}{w^2}} e^{j\left(\psi - \frac{kr^2}{2R(z)} - l\varphi - kz\right)} \times \begin{bmatrix} 1 \\ -sj \end{bmatrix}, \tag{2}$$

with p and l being the radial and azimuthal order number, while $w(z)$, k, $R(z)$, and $\psi = (2p + |l| + 1)\tan^{-1}[z\lambda/\pi w^2(0)]$ denoting the beam width, freespace wave vector, radius of curvature of the wavefront, and the Gouy phase, respectively. Obviously, both the intensity and phase profiles of the incident beam would not be uniformly distributed along a slit, and the excited plasmonic wave would consequently be deformed. Figure 1(c) is the top view (x–y plane, z~10 nm) of the excited plasmonic wave from one slit with incident LG parameters of $l = 7$ and $s = -1$. The annular intensity of the incident beam is designed to guarantee more overlap with the middle part of the slit so that the plasmonic wave has its largest intensity along the perpendicular bisector. Meanwhile, the phase front of the plasmonic wave is not parallel to the slit anymore, but is slightly tilted according to the value of l [25].

Following the well-studied spin-orbit coupling in plasmonic nanostructures [26,27], both SAM and OAM together contribute to the phase shift between plasmonic waves of two adjacent slits as

$$\Delta\phi = \phi_{i+1} - \phi_i = -\frac{l + s}{N} 2\pi, \tag{3}$$

where $\Phi_i (i = 1 \sim N, \Phi_{N+1} = \Phi_1)$ represents the phase of certain plasmonic waves. Therefore, the optical lattice is determined by both the angular momentum and the polygonal plasmonic mode as

$$\boldsymbol{E}_{\mathrm{OL}} = \sum_{i=1}^{N} \boldsymbol{E}_i e^{j\phi_i} = \sum_{i=1}^{N} \boldsymbol{E}_i e^{j\phi_1 + j(i-1)\Delta\phi}. \tag{4}$$

Following Eq. (4), the intensity pattern of the optical lattice with $l = 7$ and $s = -1$ is calculated and shown in Fig. 1(d).

It could be found that the pattern is a little deformed as the optical lattice is slightly rotated compared with the slit and occupies more intensity in the center, which is due to the inhomogeneous excitation along the slit, as illustrated in Fig. 1(c). But it is worth mentioning that SAM does not bring any aberrances to the generated optical lattice. The reason is that the circular polarization at one slit has the same decomposition basis (i.e., axes that are parallel and perpendicular to the slit). Consequently, the intensity and phase profiles of the incident LG beam do contribute to the deformation of the lattice pattern, while the polarization does not. Though the intensity decays fast beyond two lattice vector lengths from the center in Fig. 1(d), a much longer range could be achieved by using a larger device, as the deformation is only obvious near the edge of the optical lattice.

In a hexagon-shaped device, the number of possible values for $\Delta\Phi$ is $N = 6$ in Eq. (3). Optical lattices induced by all the possible values of $\Delta\Phi$ are exhaustively illustrated with $s = 1$ and $l = -1 \sim 4$ for Figs. 2(a)–2(f). It is interesting to witness the evolution of intensity pattern by simply varying the value of $\Delta\Phi$. There are totally three kinds of patterns, namely, triangle, honeycomb, and, hexagon. Though they seem quite different intuitively, these patterns are, in fact, all geometrically inherited from the original shape of the hexagon plasmonic mode. Unsurprisingly, the pattern rotation occurs and is due to the deformation of the LG beam, as discussed above.

Meanwhile, the phase profiles change dramatically. As illustrated in Fig. 2, an optical lattice with a helical phase front (i.e., the vortex lattice) is generated. In an optical vortex, there is always a phase singularity, around which the phase profile evolves from 0 to 2π periodically. The topological charge can be calculated by integrating the phase gradient along any closed path around the singularity [28]

$$Q = \frac{1}{2\pi} \oint \mathrm{d}\boldsymbol{s} \cdot \nabla\chi, \tag{5}$$

where $d\boldsymbol{s}$ is the infinitesimal displacement along the closed path and χ is the phase profile. Thus, the topological charges of vortex arrays in Figs. 2(b) and 2(c) are identified as 1 and 2, respectively, while those for Figs. 2(e) and 2(f) are opposite values of −2 and −1. In contrast, the optical lattices in Figs. 2(a) and 2(d) are completely without helicity and possess binary phase profiles everywhere in the field potential. Specifically, Fig. 2(d) is an array of cogwheel beams (azimuthally standing waves) [8].

To identify the possible vortex phenomena more intuitively, the transversal component of a Poynting vector is shown for reference (the vector length is normalized in each graph for more clarity). The rotating direction of the Poynting vector is in accord with a positive (negative) value of topological charge following the right (left) hand rule and the phase singularities exactly locate at the rotation centers. Consistent with the previous discussion, the vortex distributions are almost identically opposite when comparing Fig. 2(b) with Fig. 2(f) or Fig. 2(c) with Fig. 2(e), and the helicity is completely zero in Figs. 2(a) and 2(d). With respect to the case without helicity, the optical lattice with helicity occupies the transversal Poynting vector and proportional azimuthal linear momentum, thus carrying OAM locally [6].

As the scattering force is directly related to the energy flux [5], the helicity could be involved as a nonconservative field potential, resulting in enhanced Brownian motion of

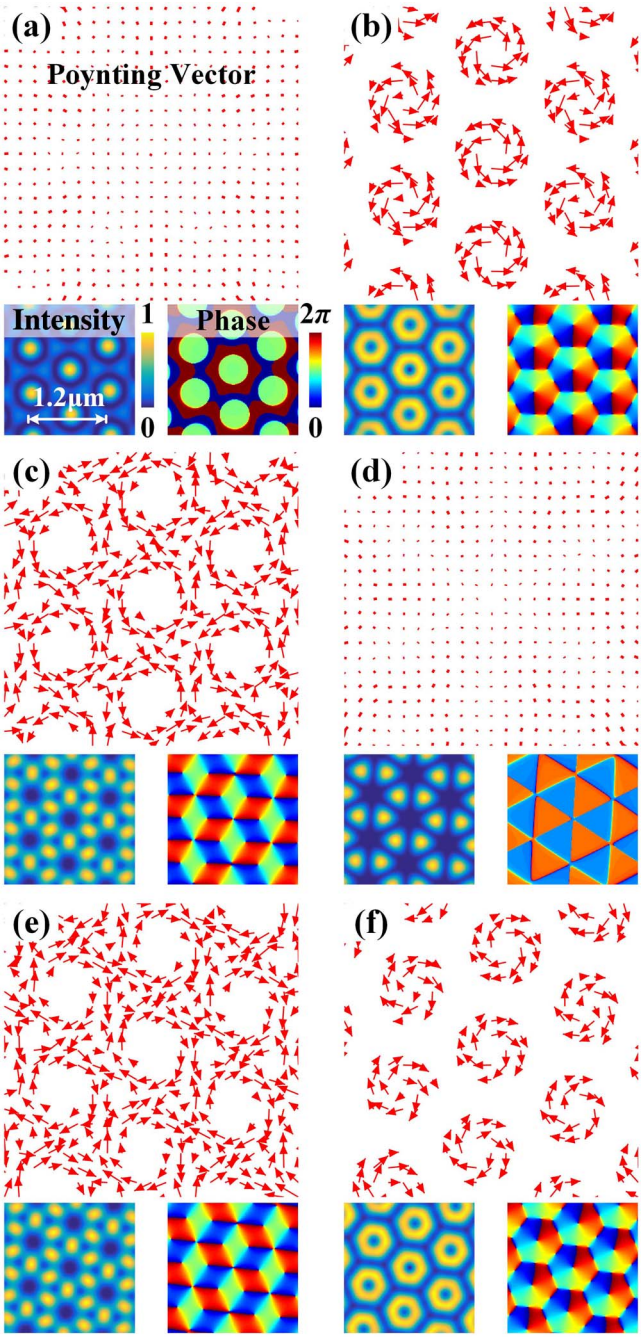

Fig. 2. Intensity patterns, phase (of $\boldsymbol{E}_z$) and Poynting vector profiles of optical lattices generated upon a hexagon-shaped device. (a)–(f) Incident beams with $s = 1$ and $l = -1 \sim 4$, in sequence. Optical lattices with and without helicity are both generated.

particles [17], which is quite useful for studying particle diffusion and even classic random walk. Though the scattering force pushes the particles along the Poynting vector, the gradient force traps and keeps them at places with maximum intensity [5]. This controllable dynamic could also be considered as a nano/microdiffuser in an integrated microfluidic system by realizing a periodic vortex potential. If a stable potential that simply traps particles is needed, the helicity could be immediately removed by simply tuning the incident beam.

Consequently, in the hexagon-shaped device, optical lattices both with and without helicity could be generated with proper $\Delta\Phi$. Specifically, an optical lattice without helicity is generated with $\Delta\Phi = 0$ or $\Delta\Phi = \pi$ and an optical lattice with helicity (i.e., the vortex lattice) can be obtained with other values of $\Delta\Phi$.

An optical lattice can be switched between one with helicity and one without helicity simply by changing incident LG beams, which is realized by varying the computer generated holograms on the spatial light modulator (SLM). As the typical refresh frequency of a SLM is ~50 Hz, the switching between different optical lattices is dynamic and nearly continuous. More details about the experimental techniques will be discussed later.

Till now, we have shown the hexagon-shaped device as a specific example. When other possible polygonal shape with various N is considered, different optical lattices could be achieved by varying both $\Delta\Phi$ and the polygonal plasmonic mode. Here, four examples with triangle ($N = 3$), square ($N = 4$), pentagon ($N = 5$), and octagon ($N = 8$)-shaped devices are shown in Fig. 3. While illuminated by the same beams ($s = 1$ and $l = 3$ for the first column and $s = 1$ and $l = -4$ for the second), $\Delta\Phi$ is determined by N as stated in Eq. (3), so that the generated optical lattices are distinct.

Unsurprisingly, all of the intensity patterns are inherited from the original shapes of the corresponding polygonal plasmonic modes as shown in four rows. Particularly, if N is even, $\Delta\Phi = 0$ or $\Delta\Phi = \pi$ still correspond to optical lattices without helicity and other values of $\Delta\Phi$ correspond to ones with helicity and phase singularities. Both the phase and Poynting vector profiles illustrate this. If N is odd, however, the helicity would always emerge despite the value of $\Delta\Phi$. Moreover, it is worth noticing that vortex with higher topological charge could be generated with a higher order of polygonal plasmonic mode. For example, the octagon plasmonic mode supports the topological charge of −3, located at the potential center.

Above all, generating an optical lattice could be summarized as follows. First, the polygonal plasmonic mode (determined by N) defines the fundamental pattern of the generated optical lattice. For instance, all of the triangle, honeycomb, and hexagon lattices in Fig. 2 are inherited from the original hexagon shape. The parity of polygonal plasmonic mode order is also critical, as an odd one could never support optical lattice without helicity. Second, the SAM and the OAM of incident beam, together with the value of N, resolve the phase difference $\Delta\Phi$ between plasmonic waves of adjacent slits. Then the intensity pattern and phase profile are determined, and optical lattices both with and without helicity can be generated with proper design. Third, the intensity and phase profile of the incident LG beam would rotate the pattern and the intensity is more centrally concentrated, as a kind of deformation.

Though only analytical results are demonstrated in this Letter, the experimental scheme should also be discussed briefly here for the sake of completeness. Our proposed device can be prepared by sputtering gold on a glass substrate and using the focused ion beam (FIB) etching process. By sequentially using a laser, a commercial SLM, and a quarter wave plate, a LG beam with arbitrary polarization state and OAM is close at hand. Then by employing an optical lens, the LG beam could be adjusted to achieve appropriate overlap with the metal slits and illuminate the back side of the membrane perpendicularly, as

shown in Fig. 1(b). As discussed above, it is feasible to experimentally achieve our proposed device [27,29]; the corresponding work is ongoing.

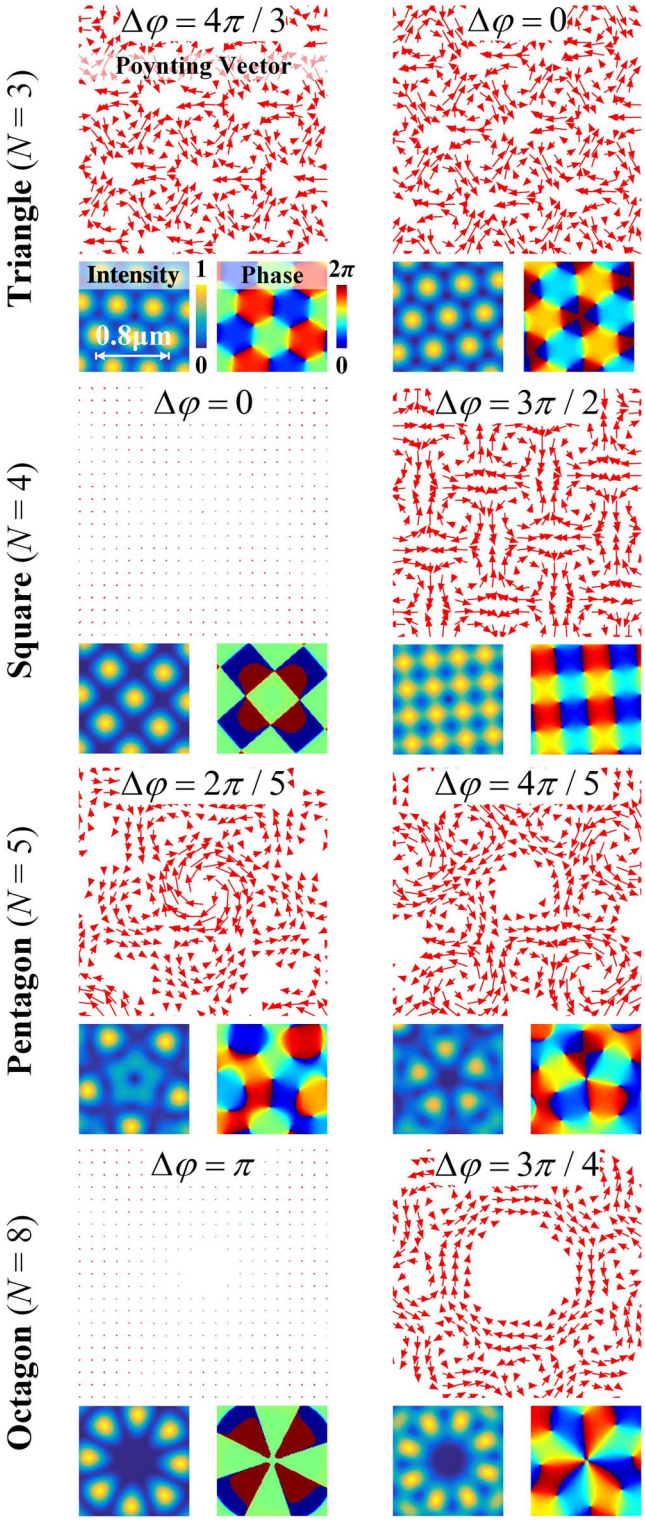

Fig. 3. Illuminated by the same beams ($s = 1$ and $l = 3$ for the first column and $s = 1$ and $l = -4$ for the second), the intensity patterns, phase (of $\boldsymbol{E}_z$) and Poynting vector profiles of optical lattices generated upon triangle ($N = 3$), square ($N = 4$), pentagon ($N = 5$), and octagon ($N = 8$)-shaped devices, respectively.

In this Letter, we have proposed an on-chip scheme to generate multipatterned optical lattices by plasmonic modes, which shows great flexibility and tunability for various possible field potential. It is inspiring to generate optical lattices with helicity or not by simply tuning the incident beam. An optical lattice with or without helicity provides a stable potential that traps, while a lattice with helicity could provide the potential for the research of classical random walk, particle Brownian motion, etc. We believe this work could provide new possibilities to manipulate on-chip optical lattices and their corresponding applications.

Funding. National Basic Research Program of China (2013CB328704, 2013CBA01704); National Natural Science Foundation of China (NSFC) (61321004); Opened Fund of the State Key Laboratory on Integrated Optoelectronics, China (IOSKL2013KF09).

REFERENCES

1. I. Bloch, J. Dalibard, and W. Zwerger, Rev. Mod. Phys. **80**, 885 (2008).
2. X. Luo, L. Wu, J. Chen, R. Lu, R. Wang, and L. You, New J. Phys. **17**, 083048 (2015).
3. I. Bloch, Nat. Phys. **1**, 23 (2005).
4. S. Safaei, C. Miniatura, and B. Grémaud, Phys. Rev. A **92**, 043810 2015).
5. M. Padgett and R. Bowman, Nat. Photonics **5**, 343 (2011).
6. M. Padgett, J. Courtial, and L. Allen, Phys. Today **57**(5), 35 (2004).
7. S. M. Barnett, J. Opt. B: Quantum Semiclassical Opt. **4**, S7 (2002).
8. Y. Wang, X. Feng, D. Zhang, P. Zhao, X. Li, K. Cui, F. Liu, and Y. Huang, Sci. Rep. **5**, 10958 (2015). doi: 10.1038/srep10958
9. D. G. Grier, Nature **424**, 810 (2003).
10. D. Zhang, X. Feng, and Y. Huang, Opt. Express **20**, 26986 (2012).
11. W. Liu, G. Chen, Y. Wang, Y. Wang, X. Feng, Y. Xie, Y. Huang, and H. Yang, IEEE Design and Test of Computers **31**, 28 (2014).
12. D. P. Ghai, S. Vyas, P. Senthilkumaran, and R. S. Sirohi, Opt. Commun. **282**, 2692 (2009).
13. J. Courtial, R. Zambrini, M. R. Dennis, and M. Vasnetsov, Opt. Express **14**, 938 (2006).
14. R. K. Singh, A. M. Sharma, and P. Senthilkumaran, Opt. Lett. **40**, 2751 (2015).
15. M. P. MacDonald, G. C. Spalding, and K. Dholakia, Nature **426**, 421 (2003).
16. K. Ladavac and D. Grier, Opt. Express **12**, 1144 (2004).
17. S. Albaladejo, M. I. Marqués, F. Scheffold, and J. J. Sáenz, Nano Lett. **9**, 3527 (2009).
18. J. Scheuer and M. Orenstein, Science **285**, 230 (1999).
19. C. J. E. Straatsma, M. K. Ivory, J. Duggan, J. Ramirez-Serrano, D. Z. Anderson, and E. A. Salim, Opt. Lett. **40**, 3368 (2015).
20. Z. Liu, Y. Wang, J. Yao, H. Lee, W. Srituravanich, and X. Zhang, Nano Lett. **9**, 462 (2009).
21. H. Raether, *Surface Plasmons on Smooth Surfaces* (Springer, 1988).
22. W.-Y. Tsai, J.-S. Huang, and C.-B. Huang, Nano Lett. **14**, 547 (2014).
23. L. Allen, M. W. Beijersbergen, R. J. C. Spreeuw, and J. P. Woerdman, Phys. Rev. A **45**, 8185 (1992).
24. A. D. Rakić, A. B. Djurišić, J. M. Elazar, and M. L. Majewski, Appl. Opt. **37**, 5271 (1998).
25. H. Zhou, Y. Zhou, J. Zhang, and J. Dong, IEEE Photon. J. **7**, 1 (2015).
26. P. Zilio, E. Mari, G. Parisi, F. Tamburini, and F. Romanato, Opt. Lett. **37**, 3234 (2012).
27. S.-W. Cho, J. Park, S.-Y. Lee, H. Kim, and B. Lee, Opt. Express **20**, 10083 (2012).
28. A. M. Amaral, E. L. Falcão-Filho, and C. B. de Araújo, Opt. Express **22**, 30315 (2014).
29. H. Kim, J. Park, S.-W. Cho, S.-Y. Lee, M. Kang, and B. Lee, Nano Lett. **10**, 529 (2010).